Numerical Analysis on Triceratops Restraining System: Failure Conditions of Tethers

Srinivasan Chandrasekaran, Manda Hari Venkata Ramachandra Rao

Abstract—Increase in the oil and gas exploration in ultra deep-water demands an adaptive structural form of the platform. Triceratops has superior motion characteristics compared to that of the Tension Leg Platform and Single Point Anchor Reservoir platforms, which is well established in the literature. Buoyant legs that support the deck are position-restrained to the sea bed using tethers with high axial pretension. Environmental forces that act on the platform induce dynamic tension variations in the tethers, causing the failure of tethers. The present study investigates the dynamic response behavior of the restraining system of the platform under the failure of a single tether of each buoyant leg in high sea states. Using the rain-flow counting algorithm and the Goodman diagram, fatigue damage caused to the tethers is estimated, and the fatigue life is predicted. Results shows that under failure conditions, the fatigue life of the remaining tethers is quite alarmingly low.

Keywords—Fatigue life, Failure analysis, PM spectrum, rain flow counting, triceratops.

I. INTRODUCTION

OFFSHORE structures are prone to various indeterministic environmental loads while the design is deterministic. The responses of the offshore platform under the imposed position-restraining systems need to be investigated in random waves. Geometric forms of offshore platforms play a significant role in effective disbursement of the encountered loads in deep waters. For example, a triangular Tension Leg Platform has a lower deck response than that of the TLP with conventional square geometry. Inspired upon the advantage of triangular geometry, new-generation platforms like offshore triceratops possess better station-keeping characteristics and improved dry-tree access with a fixed well-head. Triceratops is a novel structural form due to the presence of ball joints. Ball joints, which connect the buoyant legs to the deck, restrain the transfer of rotational motion. As a result, even for a larger response of the buoyant legs under waves, the deck remains unaffected. Both the analytical and experimental studies carried out on the stability of Buoyant Leg Structures (BLS) indicates that natural periods of pitch and roll degrees-of-freedom are well apart from that of the dominant wave period. Buoyant legs are position-restrained by pre-tensioned tethers. Seismic activities of the seabed influence the variation of pre-tension in the tethers, resulting in a significant heave

Srinivasan Chandrasekaran, Professor is with the Department of Ocean Engineering, Indian Institute of Technology Madras, Chennai, India (corresponding author phone: +91-044-22574821; fax: +91-044-22574802; e-mail: drsekaran@iitm.ac.in)

Manda Hari Venkata Ramachandra Rao, research scholar, is with the Department of Ocean Engineering, Indian Institute of Technology Madras, Chennai, India (e-mail: harichandu147@gmail.com).

response. As a result, a considerable shift is observed in the natural periods of the platform in almost all degrees-of-freedom. Free-floatation studies on the buoyant legs show higher natural periods in the surge, sway, and heave, conforming a convenient installation due to large compliance . However, the increase in the payloads cause instability in the tethers. The present study examines the triceratops proposed in the literature for its fatigue failure of tethers .

II. NUMERICAL MODELLING

The deck is modeled as a solid element, and the forces on the buoyant legs are computed using the Morison equation. The deck is connected to the buoyant leg by ball joints. Tethers connect the buoyant legs to the sea floor with high axial pretension. Table I summarizes the geometric and mass properties of the platform used in the current study.

TABLE I
DETAILS OF TRICERATOPS

Description	Values
Side of the triangular deck	95.0 m
Water depth (d)	1055.0 m
Length of tether (L_0)	900.76 m
Area of tethers	0.213E-06 m^2
The axial stiffness of tether	49.7 MN/m
No. of tethers per each leg	3
No. of buoyant legs	3
The diameter of the buoyant leg (D)	15.0
Length of buoyant leg	174.24 m
The thickness of the buoyant leg (t)	40 mm
Buoyancy per buoyant leg	274 MN
Weight of deck + payload	262 MN
Total weight of buoyant legs and tethers	209 MN
Total weight of the ballast	91.5 MN
Initial pretension in each group of tethers per leg	28.8 MN
Metacentric height of the buoyant leg	37.25 m
Distance between the mass center (CG) and center of buoyancy (COB) of buoyant leg	-37.163 m

III. METHODOLOGY

A. PM Spectrum

Ocean waves are considered to be ergodic, i.e., similar behavior when averaged over time as well as space. Such random waves are generated using the PM spectrum. The platform is subjected to different sea states and currents.

Table II shows the sea states considered for the analysis.

$$s(\omega) = \frac{1}{2\pi} \frac{H_s^2}{4\pi T_z^4} \left(\frac{2\Pi}{\omega}\right)^5 e^{\left(-\frac{1}{\pi T_z^4}\left(\frac{2\pi}{\omega}\right)^4\right)} \qquad (1)$$

TABLE II
SEA STATES

Sea States	H_s (m)	T_z (s)	U_w (m/s)
S_1	6.5	8.18	15
S_2	10	10.3	35
S_3	15	12.98	45

Current velocity, as a function of wind velocity, is considered to vary between 1-3% of that of the wind velocity. A standard three-point current velocity profile of Gulf of Mexico is considered in the study. Current velocity of intensity C_1 (= 0.16m/s) is applied in sea state s_1 and C_2 (= 1.13m/s) is applied in sea states s_2 and s_3, respectively.
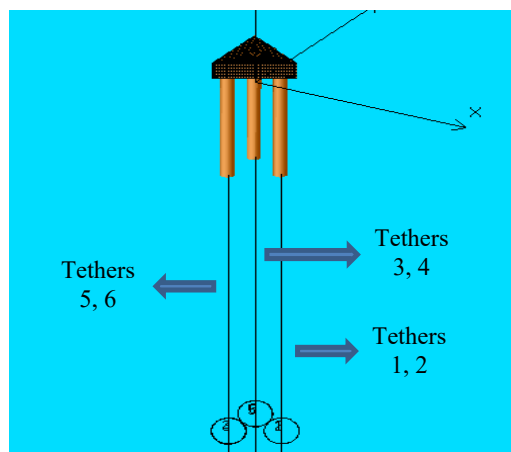
Fig. 1 Numerical Model of Triceratops

B. Rain Flow Counting

Under the wave loads, variable submergence of the buoyant legs induces variation in the axial pre-tension of the tethers. The platform is subjected to random waves, and the stress variation in tethers will also be random; it depends on the variable submergence of the buoyant legs. Rain flow counting is used to identify the cycle ranges and cycle average even for the hidden cycles of a broad-banded spectrum. The principle is to count the hysteresis loops according to the stress-strain properties.

The presence of pre-tension makes the stress response of the tether as a non-zero mean process. Hence, after obtaining the cycle ranges and cycle averages, each cycle is converted into an equivalent stress range of zero mean using the Goodman Diagram. A corresponding number of cycles that are required to cause fatigue failure is computed from the S-N curve. For the slope of the bilinear curve, m (= 3), $\log_{10}a$ (=12.081) (log N axis intercept) is valid up to a stress range of 103 MPa after which slope changes to m (=5) and influences $\log_{10}a$ (=16.081). The endurance limit is taken as 41.45 N/mm^2 at 10^8 cycles. As per Miner's rule, fatigue failure will occur when the strain energy of 'n' variable amplitude cycles is equal to 'N' constant amplitude cycles. Fatigue damage is given by:

$$FD = \sum_{i=0}^{z} \frac{n_i}{N_i} \qquad (2)$$

A member is said to be reliable only when it is capable of performing its intended function within the design life successfully. Reliability index, which is a common indicator of the probability of failure, is given by:

$$\beta = \frac{(\mu_R - \mu_S)}{\sqrt{\sigma_R^2 + \sigma_S^2}} \qquad (3)$$

μ_R - Mean Resistance (630.8 N/mm^2) ; μ_S - Mean Demand (N/mm^2); σ_R - Standard Deviation of Resistance (33.7 N/mm^2) ; σ_S – Standard Deviation of Demand (N/mm^2).

Probability of failure is obtained from the cumulative distribution function (CDF) of the standard normal distribution, which states that the chances of failure against yielding as:

$$P_f = \Phi^{-1}(-\beta) \qquad (4)$$

Φ – Standard Normal Cumulative Distribution function.
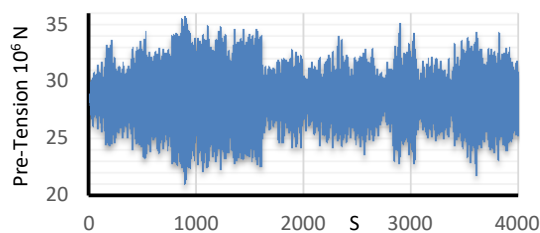
Fig. 2 Response of the tether 1 before failure in sea state S_1
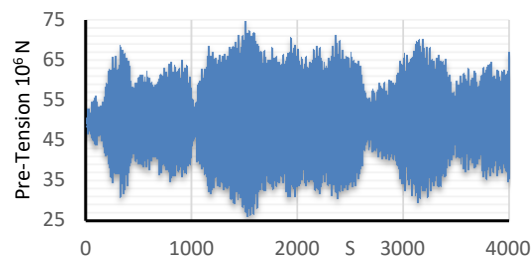
Fig. 3 The response of the tether 1 after the failure in sea state S_1

TABLE III
CONDITIONS AFTER FAILURE OF TETHERS

S. No	Properties	Before the failure of 3 tethers	After the failure of 3 tethers
1	Total weight of Triceratops	565.5	518.59
2	Stiffness of restraining system (MN/m)	447.3	298.2
3	Pre-Tension per tether (MN)	28.8	49.6

IV. RESULTS AND DISCUSSION

Failure of each tether under a single buoyant leg has decreased the stiffness of the platform restraining system. The change in stiffness of the restraining system is seen as 33.33%

and reduced the weight considerably by 7%. While the initial pretension under no-failure condition is about 28 MN, post-failure compels the remaining tethers to share this pretension. It results in an increase of about 72% in each tether. Table III summarizes the details of the platform before and after the failure of the tethers. Fig. 2 shows the response under normal condition in sea state S_1 and Fig. 3 shows the response of the tether 1 in the sea state S_1 after the failure of three tethers. From Figs. 2 and 3 it is observed that the variation of tension in tethers is 10 and 30 MN respectively.

symmetric and not heavily tailed as the mean, median, and mode are equal in all the cases, conforming to a normal distribution.

TABLE IV
NATURAL PERIODS AND DAMPING RATIOS

DOF	Before the failure of 3 tethers		After the failure of 3 tethers	
	Period (s)	Damping ratio (%)	Period (s)	Damping ratio (%)
Surge	133.8	0.59-1.59	129.03	1.10-4.80
Sway	133.8	0.29-1.59	128.02	0.23-2.71
Heave	2.2	0.43-1.4	2.56	0.03-0.18
Roll	3.12	0.02-0.12	3.75	0.025-0.169
Pitch	3.14	0.08-0.91	3.69	0.025-0.0769
Yaw	169.07	0.43-4.45	150.43	1.9-4.28

Natural periods and damping ratios are obtained by free-decay test, using the logarithmic decrement method. Table IV shows the values of natural periods and the range of the corresponding damping ratios. It is seen that there is a decrease in the natural periods in complaint degrees-of-freedom while a marginal increase is noticed in the stiff degrees-of-freedom. Tables V-VII show the descriptive statistics of the stress process. It is seen that they are

TABLE V
DESCRIPTIVE STATISTICS OF TETHER 1

Sea States	μ_x	$\tilde{x}$	Mode	σ	γ (10^{-3})	K_4 (10^{-1})
S_1	233.7	233.6	233.7	34.9	-2.3	-3.57
S_1+C_1	233.7	233.8	230.3	31.5	-6.3	-5.14
S_2	233.7	233.7	233.7	42.5	-0.19	-9.40
S_2+C_2	233.8	233.6	233.8	39.6	11.14	-2.34
S_3	233.6	233.6	233.7	34.9	-0.86	-3.10
S_3+C_2	233.7	233.7	233.8	45.8	-0.51	-4.46

TABLE VI
DESCRIPTIVE STATISTICS OF TETHER 3

Sea States	μ_x	$\tilde{x}$	Mode	σ	γ (10^{-3})	K_4 (10^{-1})
S_1	232.6	232.6	226.4	24.7	-4.4	-5.3
S_1+C_1	232.6	232.6	240.9	25.6	-1.6	-7.9
S_2	232.5	232.4	232.3	22.5	-0.77	-7.2
S_2+C_2	232.6	232.5	232.5	28.0	4.2	-4.4
S_3	232.5	232.4	237.3	18.4	24.9	-2.4
S_3+C_2	232.5	232	233	23.8	29.5	-3.5

TABLE VII
DESCRIPTIVE STATISTICS OF TETHER 5

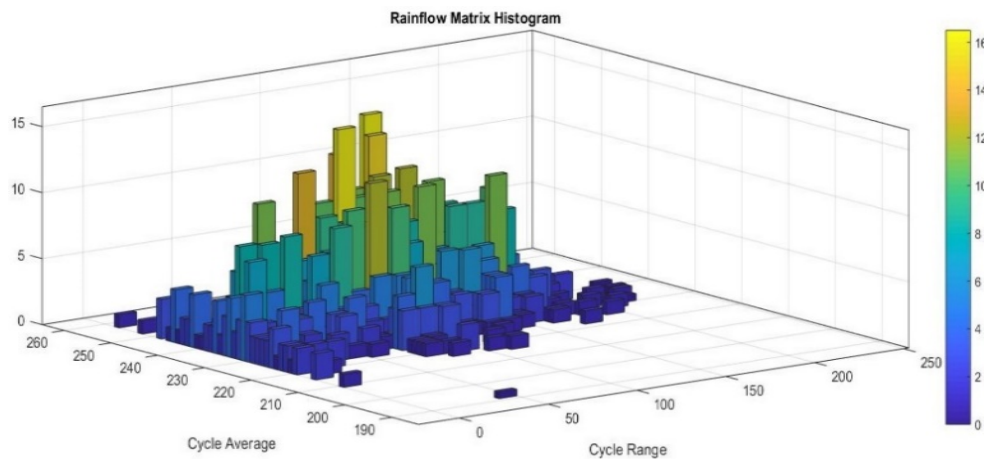| Sea States	μ_x	$\tilde{x}$	Mode	σ	γ (10^{-3})	K_4 (10^{-1})
S_1	232.6	232.6	232.6	24.7	-4.4	-5.4
S_1+C_1	232.6	232.6	232.6	25.9	-1.6	-8.0
S_2	232.5	232.5	232.6	22.3	-1.0	-7.7
S_2+C_2	232.6	232.5	232.5	27.5	-4.6	-4.4
S_3	232.5	232.4	232.6	18.1	-25.6	-2.3
S_3+C_2	232.5	232.4	240.6	23.5	-30.6	-3.9

Fig. 4 Rainflow counting matrix of tether 1 in sea state S_1

From Fig. 4, the maximum stress cycle range is about 225 N/mm² with a mean stress of 230 N/mm² approximately. The stress cycle ranges are varying between 0-225 N/mm², and the cycle average is varying between 210-260 N/mm².

It is seen from Fig. 5 that the stress cycle ranges of tether 3 are varying about 0-140 N/mm² and the cycle average are varying in between 220-250 N/mm². The cycle ranges and cycle averages of the tether 1 are more than that of tether 3.
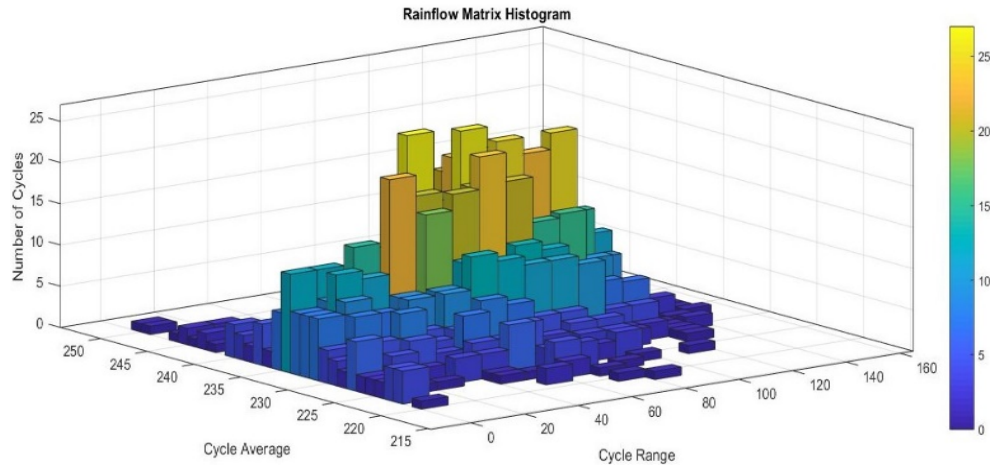
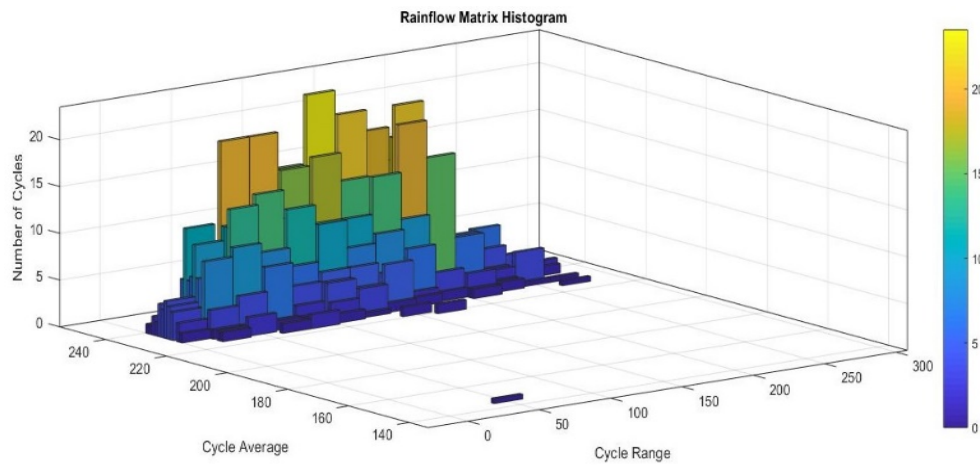Fig. 5 Rainflow counting matrix of tether 3 in sea state S_1

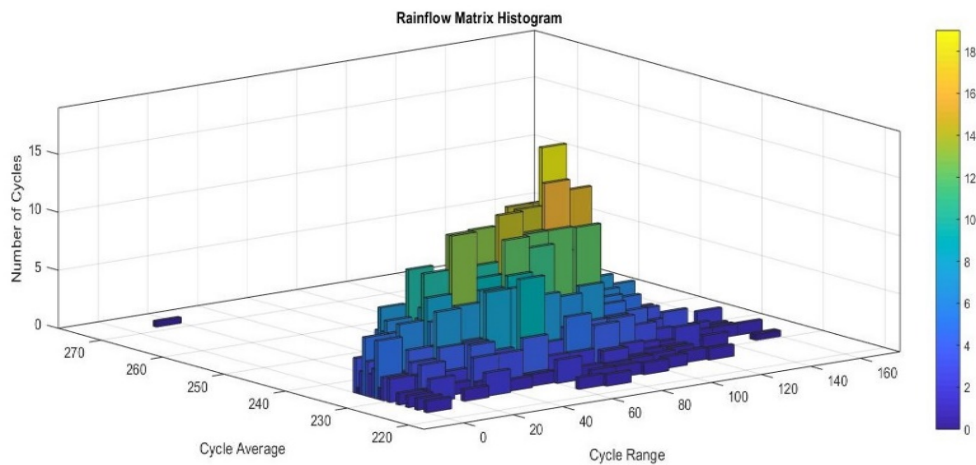Fig. 6 Rainflow counting matrix of tether 1 in sea state $S_3 + C_2$

Fig. 7 Rainflow counting matrix of tether 3 in sea state $S_3 + C_2$

It is seen from Fig. 6 that the cycle ranges are reaching up to 270 N/mm^2 while the cycle average in more concentrated at 240 N/mm^2.

It is seen from Fig. 7 that the cycle ranges are approaching a value of 160 N/mm^2 and cycle averages are concentrated at 230 N/mm^2. As the mean and standard deviation of the stress

process is high, the reliability index against yielding values is relatively lesser than that of the normal condition. It indicates an increase in the probability of failure. The reliability index against yielding values are computed and summarized in Table VIII in the range of (6.9768-10.4004) having a probability of failure of ($1.51*10^{-12}$-$1.234*10^{-25}$).

TABLE VIII
RELIABILITY AND FATIGUE LIFE

	Parameters	S_1	S_1+c_1	S_2	S_2+C_2	S_3	S_3+C_2
Tether 1	Fatigue life (years)	0.03	0.04	0.02	0.02	0.03	0.01
	β_{yield}	8.18	8.59	7.31	7.63	8.18	6.97
Tether 3	Fatigue life (years)	0.09	0.07	0.18	0.05	0.34	0.12
	β_{yield}	9.51	9.39	9.81	9.08	10.3	9.64
Tether 5	Fatigue life (years)	0.09	0.07	0.20	0.06	0.36	0.12
	β_{yield}	9.52	9.40	9.84	9.14	10.4	9.69

V. CONCLUSION

Fatigue failure of offshore triceratops under different sea states in the presence of waves and currents is examined. Dynamic response of buoyant legs caused tether tension variation in pre-tensioned tethers. Following conclusions are drawn:

a) The Pre-Tension developed in the tethers shifts to higher values from initial value.

b) As the stiffness of the platform restraining system reduces, the standard deviation of the stress variation is higher.

c) The fatigue life of the tethers reduces significantly.

The presented study shows the importance of the restraining system in health monitoring as an important future scope of research as well.

REFERENCES

[1] S. Chandrasekaran and A. K. Jain, "Dynamic behavior of the square and triangular offshore tension leg platforms under regular wave loads," *Ocean Engineering,29(3),* pp. 279-313, 2002.

[2] C. N. White, R. W. Copple and C. Capanoglu, "Triceratops: an effective platform for developing oil and gas fields in deep and ultra-deep water.," in *The fifteenth international offshore and polar engineering conference. International society of offshore and polar engineers*, Seoul, 2005.

[3] S. Chandrasekaran and M. Seeram, "Stability studies on an offshore triceratops," *International Journal of Innovative Research and Development. (ISSN 2278–0211),* vol. 1(10), pp. 398-404., 2012.

[4] S. Chandrasekaran and M. Nannaware, "Response analyses of the offshore triceratops to seismic activities," *Ships and Offshore Structures,* vol. 9(6), pp. 633-642, 2013.

[5] S. Chandrasekaran, S. Mayank, and A. Jain, "Dynamic Response Behaviour of Stiffened Triceratops Under Regular Waves: Experimental Investigations," in *In ASME 2015 34th International Conference on Ocean, Offshore and Arctic Engineering*, 2015, May.

[6] S. Chandrasekaran and S. Madhuri, "Dynamic response of offshore triceratops: Numerical and Experimental investigations," *Ocean Engineering,* pp. 109, 401-409, 2015.

[7] S. Chandrasekaran and P. A. Kiran, "Mathieu stability of offshore triceratops under postulated failure," *Ships and Offshore Structures,* pp. 13(2), 143-148, 2018.

[8] S. Chandrasekaran and R. Nagavinodini, "Dynamic analyses and preliminary design of offshore triceratops in ultra-deep waters," *Innovative Infrastructure Solutions,* pp. 3(1), 16, 2018.

[9] D. V. Reddy and A. Swamidas, Essentials of Offshore Structures: Framed and Gravity Platforms, Boca Raton, CRC Press, 2013.

[10] "Interim Guidance on Hurricane Conditions in the Gulf of Mexico," May2007.(Online).Available: https://law.resource.org/pub/us/cfr/ibr/002/api.2int-met.2007.pdf.

[11] Veritas and D. N., Fatigue design of offshore steel structures. DNV Recommended Practice, DNVGL - RP-C203,20, 2010.

[12] Adam. J. Sadowski, J. Michael Rotter, Thomas Reinke and Thomas Ummenhofer, "Statistical analysis of the material properties of selected structural carbon steels," *Structural Safety,* pp. 53, 26-35. 10.1016/j.strusafe.2014.12.002., 2015.